Contents lists available at ScienceDirect

Nano Energy

Full paper

New insight into atomic-scale engineering of electrode surface for long-life and safe high voltage lithium ion cathodes

Sixu Deng[a,b,1], Biwei Xiao[a,1], Biqiong Wang[a], Xia Li[a], Karthikeyan Kaliyappan[a], Yang Zhao[a], Andrew Lushington[a], Ruying Li[a], Tsun-Kong Sham[c], Hao Wang[b,*], Xueliang Sun[a,*]

[a] Department of Mechanical and Materials Engineering, University of Western Ontario, London, Ontario, Canada N6A 5B9
[b] The College of Materials Science and Engineering, Beijing University of Technology, Beijing 100124, PR China
[c] Department of Chemistry, University of Western Ontario, London, Ontario, Canada N6A 5B7

A B S T R A C T

Spinel LiNi$_{0.5}$Mn$_{1.5}$O$_4$ (LNMO) is a promising high voltage cathode material for lithium ion batteries (LIBs). However, dissolution of Mn and unwanted side reactions between LNMO and the electrolyte raises several safety issues while also resulting in deteriorated electrochemical performance of LIBs at high working voltages. Here, we report the use of ultrathin atomic layer deposited (ALD) AlPO$_4$ thin film as a coating material for LNMO electrodes to circumvent the stated issues. The as-prepared AlPO$_4$ coated LNMO demonstrates excellent capacity retention with prolonged cycle life compared to the bare one. Synchrotron based X-ray spectroscopy was employed to understand how ultrathin coating layer improve the cycle life, and then develop a detailed mechanism for the effect of coating layer. Our studies revealed that using atomic scale coating layer with improved thermal stability effectively impede the side-reactions occurrence at high voltage, resulting in significantly improved safety and electrochemical performances.

1. Introduction

Spinel LiNi$_{0.5}$Mn$_{1.5}$O$_4$ (LNMO) is considered as a promising high voltage cathode material for use in next generation lithium ion batteries (LIBs) due to its high operating voltage plateau (about 4.7 V vs. Li$^+$/Li) and theoretical specific capacity of 147 mA h g^{-1}, effectively improving the energy density of batteries for use in electric vehicles (EVs) [1–3]. However, using such high voltage (beyond 4.5 V) exceeds the voltage window of conventional carbonate based LiPF$_6$ electrolytes, leading to rapid electrolyte decomposition and unwanted side reactions occurring between the active electrode and the electrolyte species [4–6]. Furthermore, high voltage charging process results in exothermic reactions occurring between the flammable electrolyte and metastable Li$_x$NiMnO, raising overheating symptom of batteries and triggering a number of safety hazard [7–9]. Meanwhile, decomposition of electrolyte causes the formation of an insulating solid electrolyte interphase (SEI) layer, thereby impeding Li$^+$ diffusion during the charge/discharge process, leading to serious capacity fading [2,3,10,11]. Furthermore, dissolution of Mn is another serious issue of LNMO, which causes destroyed material structure and reduced cycle life of LNMO [12–14].

To address these challenges, many strategies have been employed to improve the electrochemical performances of LNMO-based batteries, including morphology control, element doping and surface modification [15–18]. Among the available strategies, application of a surface coating is considered as an effective method for providing a stable interface between the active material and electrolyte. A number of coating materials have been employed for use on LNMO, including metal oxides (Al$_2$O$_3$ [19], ZnO [20], SiO$_2$ [21], ZrO$_2$ [22], Y$_2$O$_3$ [23]), fluorides (BiOF [24]) and metal phosphates (Li$_3$PO$_4$ [25], FePO$_4$ [26]). These coating materials aim to prevent side reactions and dissolution of metal ions to improve performances. Among them, AlPO$_4$ has been considered as a safe coating materials providing improved thermal stability [7,8], and has been widely applied as a coating for other cathode materials (e.g., Li[Li$_{0.2}$Fe$_{0.1}$Ni$_{0.15}$Mn$_{0.55}$]O$_2$ [27], LiNi$_{0.8}$Co$_{0.1}$Mn$_{0.1}$O$_2$ [28] and LiNi$_{0.8}$Co$_{0.2}$O$_2$ [29]). Cho et al. reported that LiCoO$_2$ particles coated with AlPO$_4$ dramatically reduced the heat evolution in the charged state [30–32]. The high electronegativity of PO$_4$$^{3-}$ with Al^{3+} ions enables to effectively resist the reaction between electrode materials and electrolyte, which both enhances the safety and improves the electrochemical performances of cells [32–34].

Various methods had been adopted to coat cathode with AlPO$_4$,

---

* Corresponding authors.
E-mail addresses: haowang@bjut.edu.cn (H. Wang), xsun@eng.uwo.ca (X. Sun).
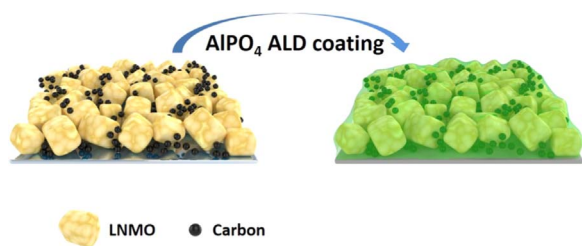[1] Sixu Deng and Biwei Xiao contribute equally to this work.

Fig. 1. Schematic diagram of $AlPO_4$ coating on LNMO electrode via atomic layer deposition.

including sol-gel [35] or wet-chemical [36] techniques. However, these coating approaches have limited control over surface coverage, thickness and uniformity. Unlike other surface modification methods, atomic layer deposition (ALD) is a novel coating technique used for the deposition of highly conformal and uniform layers with well controlled thickness [37–40]. In our group, ALD coatings such as $LiTaO_3$ and $FePO_4$ have been used on various cathode materials including $LiNi_{1/3}Co_{1/3}Mn_{1/3}O_2$ (NMC) [41] and LNMO [42]. Al_2O_3 ALD coating on the surface of LNMO is the most studied coating material, and has been shown to suppress side reactions from occurring between the electrode and the electrolyte as well as mitigating decomposition of the SEI. Kim et al. demonstrated that LNMO electrode coated with Al_2O_3 can dramatically suppress self-discharge effects as well as dissolution of transition metals [19,43]. Comparing with Al_2O_3, $AlPO_4$ coating is expected to improve both reliability and electrochemical performance of LNMO cathodes at high voltages.

For the first time, we reported the use of ultrathin $AlPO_4$ coating on high voltage LNMO electrodes via ALD (shown in Fig. 1). Cycling stability and rate capability of as-prepared LNMOs, with detailed electrochemical mechanisms, will be discussed through the use of a series of electrochemical characterization techniques. More importantly, synchrotron based X-ray studies are determined to understand the coating effect of ALD $AlPO_4$ on LNMO. It has been demonstrated that the coating layer with improved thermal stability provides a stable interface for LNMO and can effectively prevents the occurrence of side-reactions and dissolution of Mn, resulting in an improved electrochemical performance of Li-ion batteries. Our study also focus on a correlation between coatings thickness and electrochemical performances.

2. Experimental

2.1. Preparation of LNMO electrodes

Commercial LNMO powder was purchased from Daejung Energy Materials Co., Ltd., South Korea. Electrodes were prepared by casting a slurry of commercial LNMO, acetylene black (AB) and polyvinylidene fluoride (PVDF) in N-methyl-pyrrolidone (NMP) on aluminum foil and dried at 80 °C under vacuum overnight. The weight ratio of active material: AB: PVDF was 8: 1: 1.

2.2. Preparation of ALD $AlPO_4$ coated LNMO electrodes

Amorphous aluminum phosphate ($AlPO_4$) was deposited on LNMO electrodes at 250 °C using trimethyl phosphate [TMPO, $(MeO)_3PO$], trimethylaluminium (TMA) and water (H_2O) as precursors in a Savannah 100 ALD system (Cambridge Nanotech, USA). Source temperature for TMPO was 75 °C while TMA and H_2O were held at room temperature (RT). The deposition was achieved by following a sequence of TMPO (2 s pulse)- purge (10 s)- H_2O (0.5 s pulse)- purge (15 s)- TMA (0.5 s) pulse- purge (10 s)- H_2O (0.5 s pulse)- purge (15 s). Nitrogen gas (99.999%) was used as a carrying and purging gas at a flow rate of 20 sccm. The thickness of the $AlPO_4$ thin film was controlled by varying the cycle numbers (n) by repeating the above

procedure. Commercial LNMO cathode electrodes were coated using 2, 5, 10, 20 and 50-ALD cycles of $AlPO_4$ (denoted as AlP-n).

2.3. Characterization

X-ray power diffraction (XRD) measurements were carried out on a Bruker D8 Advance Diffractometer (Cu-Ka source, 40 kV, 40 mA). Raman spectroscopy was performed using a HORIBA Scientific LabRAM HR Raman microscope with an excitation wavelength of 532.4 nm generated by an argon laser. The morphologies and structures of bare and $AlPO_4$ coated LNMO was observed using a field emission scanning electron microscopy (FESEM, Hitachi S4800), transmission electron microscopy with elemental mapping images (TEM, Hitachi H-7000), and high-resolution transmission electron microscopy (HRTEM, JEOL 2010F). All synchrotron X-ray studies were carried out at the Canadian Light Source (CLS). X-ray absorption near edge structure (XANES) measurements using total electron yield (TEY) was carried out on the high resolution Spherical Grating Monochromater (SGM) beamline equipped with a 45 mm planar undulator and three gratings with a photon energy range of 250–2000 eV. X-ray photoemission spectroscopy (XPS) was performed at the variable line spacing plane grating monochromator (VLS PGM) beamline at 200 eV photon energy with a total resolution of 100 meV. For differential scanning calorimetry (DSC) measurements, cells were charged to 5.0 V and held at that voltage for 2 h. After disassembling the cells, the positive electrodes were scraped from the aluminum current collector. Approximately 5 mg of the positive electrode was hermetically sealed in a stainless steel pan. The data were acquired using a TA instrument (SDT Q600) in a nitrogen atmosphere at a heating rate of 5 °C min^{-1}.

2.4. Electrochemical measurements

CR2032 coin cells were assembled in an argon-filled glove-box using lithium metal as the counter electrode and Celgard K2045 as the separator. The electrolyte was composed of 1 M $LiPF_6$ dissolved in ethylene carbonate (EC)-dimethyl carbonate (DMC) with a volume ratio of 1: 1. Cyclic voltammetry (CV) experiments were studied using a Bio-logic multichannel potentiostat 3/Z (VMP3) with a scanning rate of 0.1 mV s^{-1} and at a potential range of 3.5–5.0 V (vs Li$^+$/Li). Electrochemical impedance spectroscopy (EIS) tests were measured between the frequency range of 0.01 Hz to 100 kHz by versatile multichannel potentiostat 3/Z (VMP3). Charge/discharge tests were carried out on Arbin BT2000 with a voltage range of 3.5–5.0 V.

3. Results and discussion

X-ray-diffraction patterns of bare LNMO and AlP-50 are shown in Fig. 2a. All the reflections are well indexed basis on the cubic spinel structure of LNMO and lack any indication of rock-salt impurity phases. No peaks of $AlPO_4$ can be observed in the XRD pattern of AlP-50 because of the ultrathin and amorphous nature of ALD $AlPO_4$ coating. As can be seen from Raman spectra in Fig. S1, all LNMO samples (bare and $AlPO_4$ coated LNMO) show a strong peak at 164 cm^{-1} indication all samples follow an ordered phase $P4_332$ space group [44–46]. The peak at 638 cm^{-1} is assigned to symmetric Mn-O stretching of the MnO_6 octahedra, and two peaks around 496 cm^{-1} and 407 cm^{-1} are associated with the Ni^{2+}-O stretching mode in the structure [47]. Compared with bare LNMO, the Ni-O and Mn-O vibrations of $AlPO_4$ coated LNMO show gradual blue shifts with the increase of ALD cycles. This may be due to the $AlPO_4$ layer on the surface of LNMO restricted vibration of Ni-O and Mn-O bonds, leading to higher vibrational wavenumbers [48]. The surface morphology of the as-prepared LNMOs was characterized via FESEM (Fig. S2). Interestingly, surface of LNMO becomes gradually rougher with increased number of ALD cycles. A high-resolution TEM image of
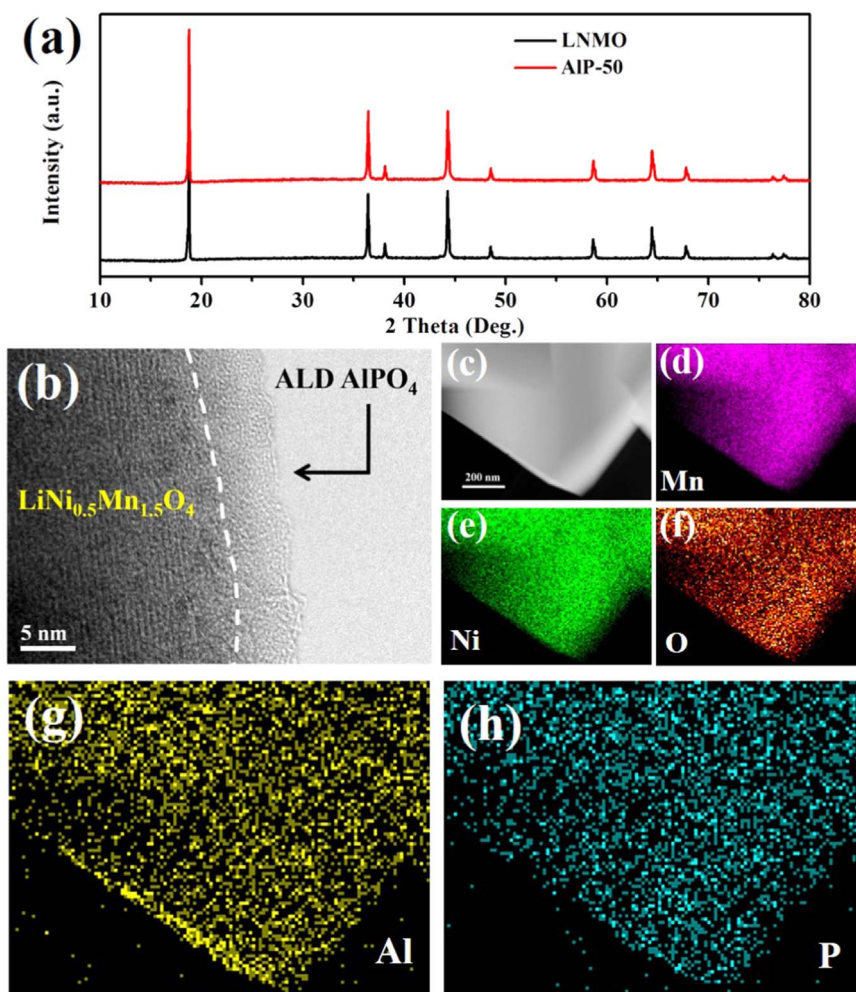
Fig. 2. (a) XRD patterns of LNMO and AlP-50; (b) HRTEM image; (c-h) EDX elements mapping of AlP-50.

AlP-50 is shown in Fig. 2b, which exhibits an amorphous and uniform layer with thickness of approximately 5 nm on the surface of the crystalline LNMO. This ultrathin and uniform layer will effectively segregate electrodes from electrolyte in order to impede side reactions. Energy dispersive X-ray spectroscopy (EDX) mapping for elements Al and P (Fig. 2g and h) demonstrates equal distribution as elements Ni, Mn and O, further indicating the uniform nature of ALD deposited $AlPO_4$.

The electrochemical performance of bare and $AlPO_4$-coated LNMO was evaluated to demonstrate the impact of $AlPO_4$ coating layer on the stability of LNMO. Ten ALD-cycles of $AlPO_4$ coating sample (denoted as AlP-10) exhibits best cycling and rate capacity. Fig. 3a shows the charge/discharge profiles of the first and 100th cycles of bare LNMO and AlP-10 at 0.5 C, respectively. The two samples exhibit discharge plateaus at about 4.7 V, corresponding to reduction of Ni^{4+}/ Ni^{3+}/ Ni^{2+}. Compared to bare LNMO, $AlPO_4$ coated sample demonstrates decreasing initial discharge capacity. After 100 cycles, the bare LNMO sample displays a significantly increased potential gap between charge and discharge plateaus. This obvious polarization is due to severe side reactions that have occurred between the active cathode material and electrolyte species. In comparison, the charge and discharge curves of AlP-10 maintains a stable plateau with minimal polarization, which can be attributed to the good protection of $AlPO_4$ coating. Cycling stability at 0.5 C of bare LNMO and AlP-10 are shown in Fig. 3b. Bare LNMO delivers higher initial discharge capacity of 115.1 mA h g^{-1}, but decays rapidly after 100 cycles, retaining 69% of its initial capacity. Impressively, AlP-10 demonstrates very stable cycling performance with high capacity retention of over 94% in the 100th cycle. The

coulombic efficiency is shown in Fig. S6. The initial coulombic efficiency decrease with the increase of ALD cycles, lower than uncoated one. We proposed that lithium may react with $AlPO_4$ layer in initial cycle, which will consume some Li and thus decrease coulombic efficiency [42]. In the following cycles, the coulombic efficiency of AlP-10 displays a stability of over 96% during cycling. This improvement is attributed to thermal stability of the uniform $AlPO_4$ protecting layer and its ability to suppress side-reactions between the cathode and electrolyte. Cycle performances of various thickness of $AlPO_4$ coating are also conducted in Fig. S3 and Fig. S5. As-prepared AlP-20 shows the lowest discharge capacity of 77.9 mA h g^{-1} (Fig. S3). This phenomenon may be ascribed to the increased electrical resistance by the insulated surface $AlPO_4$ coating layer.

Fig. 3c compares the discharge capacities between bare and $AlPO_4$-coated LNMO samples, with the C rate increasing from 0.1 to 5.0 C and then back to 0.1 C. As-prepared AlP-10 shows the higher capacity under each current densities which were 70 mA h g^{-1} at 2 C and 50 mA h g^{-1} at 5 C. Meanwhile, AlP-10 also displays excellent reversibility when the current density is reverted to 0.1 C, displaying a high specific capacity of 110 mA h g^{-1}. To understand the effect of $AlPO_4$ ALD coating, EIS of bare and $AlPO_4$ coated LNMO were tested after 100 cycles. The obtained Nyquist plots and fitted equivalent circuits are shown in Fig. 3d. Each spectrum consists of two overlapped semicircles at high to middle frequency, corresponding to the resistance of the solid electrolyte interface (R_{SEI}) and charge transfer resistance (R_{ct}), respectively [35,49,50]. In addition, the slope at the low frequency region is attributed to Warburg impedance, which is related to the lithium-ion diffusion through LNMO. The values of the R_{SEI} and R_{ct} are summarized in Table S1. EIS results
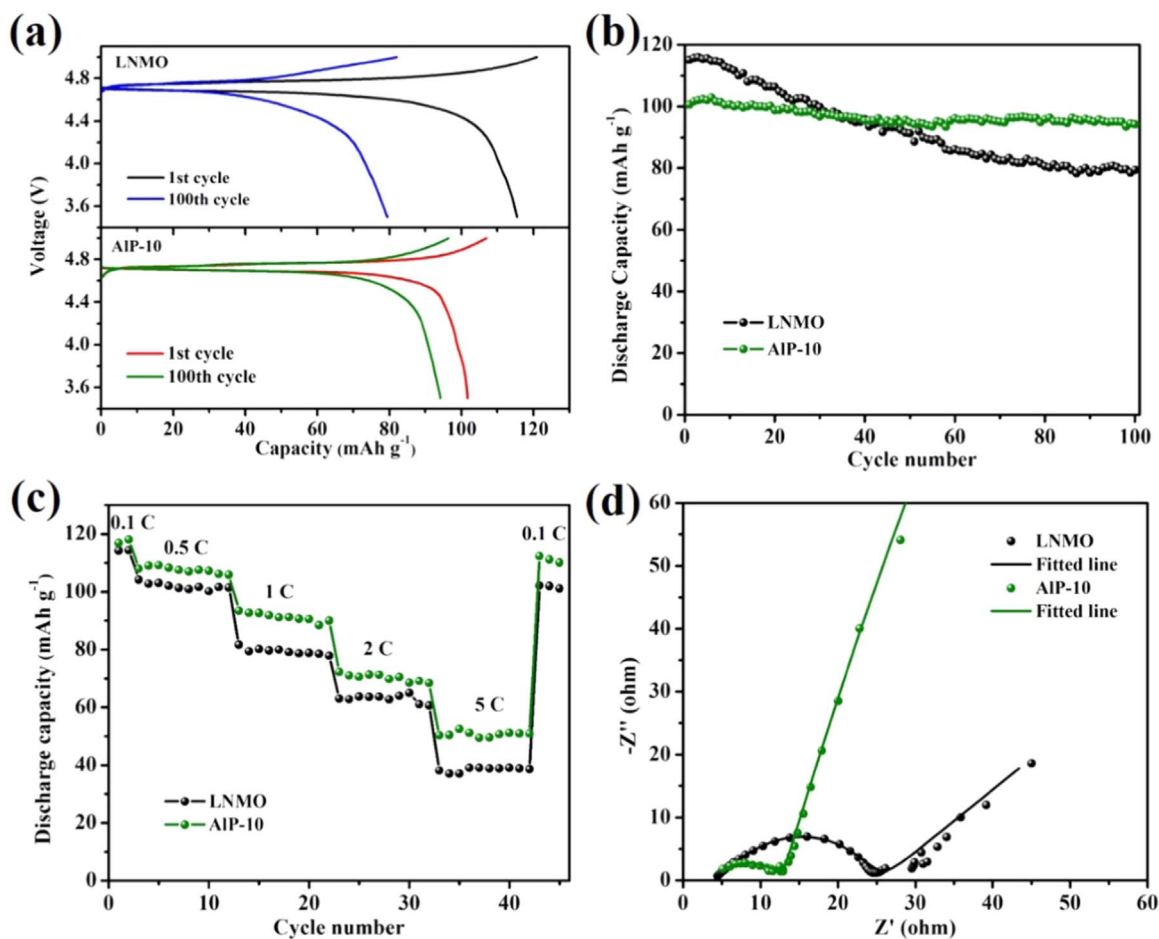
Fig. 3. (a) First and 100th cycle charge/discharge curves; (b) cycling stability; (c) rate capabilities and (d) electrochemical impedance spectra (EIS) of bare and AlPO₄ coated LNMO.

illustrate how the AlPO₄ coating on LNMO results in a smaller R_{SEI} compared to bare LNMO, indicating the protective nature of AlPO₄ to suppress unwanted side-reactions during cycling.

Cyclic voltammograms of as-prepared samples are determined in Fig. 4. Clearly, a pair of redox peaks at around 4.7 V can be observed corresponding to the oxidation and reduction reactions of Ni^{2+}/Ni^{3+} and Ni^{3+}/Ni^{4+}. No redox peaks appear at 4.0 V, indicating LNMO samples are mostly in the phase of ordered $P4_332$, agreeing with the Raman results presented earlier. The redox peaks of AlP-10 maintains the same potential compared to bare LNMO, which indicates that Li-ions penetrate smoothly through the AlPO₄ coating layers.
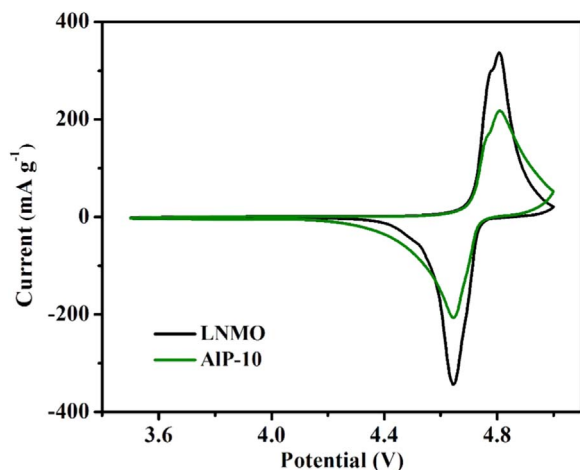

Fig. 4. Cyclic voltammograms at 0.1 mV s⁻¹ of bare and AlPO₄ coated LNMO.

Fig. 5 shows a comparison of the long cycling performance of bare LNMO and AlP-10 at 0.5 C for over 350 cycles to demonstrate the cycle stability and coating life of AlPO₄ coated LNMO. As-prepared AlP-10 exhibits an initial specific capacity of 100.6 mA h g⁻¹, and the electrode keeps a long and stable cycle life with highly reversed capacity of 75.3 mA h g⁻¹ after 350 cycles, demonstrating a high capacity retention of 74.9%. The capacity decay was only 0.07 mA h g⁻¹ per cycle. However, the initial discharge capacity of bare LNMO is 116.3 mA h g⁻¹, and decreases to 52.5 mA h g⁻¹ following 350 cycles displaying a capacity retention of 45.1%. The capacity decay of bare LNMO was 0.18 mA h g⁻¹ per cycle, which is 2.6 times compared to AlPO₄ coated sample. Furthermore, the coulombic efficiency of coated LNMO maintains at 95–97% during 350 cycles. These results further illustrate the significantly improved capacity and prolonged cycle life of LNMO with the support of AlPO₄ ALD coating.

In order to investigate the AlPO₄ coating effect on the structure of LNMO, synchrotron based Mn $L_{3,2}$-edges and O K-edges XANES spectra of bare and coated LNMOs before and after cycling were collected using total electron yield mode (TEY), as shown in Fig. 6. TEY mode collects electrons excited from the core level of the element, resulting from self-absorption of the electrons from the bulk of the material. The TEY mode manifests information from the surface region with a depth of ~5 nm [42]. As illustrated in Fig. 6a, bare LNMO and AlP-10 share the same features of $Mn^{4+}(MnO_2)$, indicating that the ALD coating process did not change valence of Mn on the surface of LNMO. Following charge/discharge cycling, bare LNMO demonstrates a high ratio of Mn^{2+} peaks, indicating that the surface structure of LNMO has been destroyed after cycling. On the contrary, AlP-10 still maintains predominantly Mn^{4+} features with a tiny Mn^{2+} peak at 640.4 eV after cycling, meaning that the Mn^{2+} evolution is effectively
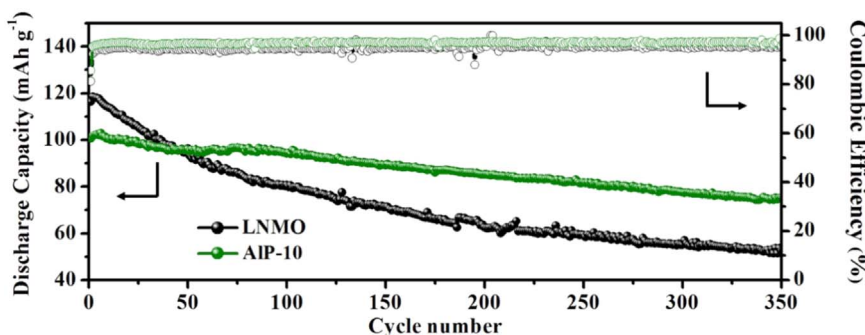
Fig. 5. Long cycling performances and coulombic efficiency of bare LNMO and AlP-10 over 350 cycles under 0.5 C.

suppressed by ALD coating. It has been reported that the reduction of Mn are always accompanied with the oxidation of electrolyte, and the reduced Mn^{2+} is well-known to dissolve into the electrolyte easily and deposit on the anode part [51–54]. Therefore, as shown in Mn $L_{3,2}$-edges results, the suppression of Mn^{4+} reduction on the surface of LNMO illustrates that the coating layer as a stable interface protects LNMO electrode materials against TMs reduction and dissolution as well as reliefs the electrolyte decomposition.

Fig. 6b presents the O K-edge XANES spectra of as-prepared LNMOs before and after cycling, providing information pertaining to oxygen-metal interaction. For bare LNMO sample, the sharp peaks at 529.7 and 532.1 eV (corresponding to peaks a and b) are related to the hybridization of unoccupied O-2p with transition metal (Ni and Mn) 3d orbitals [55,56]. Interestingly, AlP-10 shows two enhanced peaks at 532.1 (peak b) and 534.8 eV (peak c), which can be attributed to the ALD $AlPO_4$ coating layer [57]. After cycling, peak b is barely visible from the bare LNMO, indicating possible dissolution of elemental Mn and destructive structure of LNMO without any surface protection. Impressively, the spectrum for cycled AlP-10 still maintain sharp peak b and shoulder peak c, strongly demonstrating the protective ability of $AlPO_4$ during cycling. However, the peak intensity of peaks b and c from $AlPO_4$ coating layer is reduced following cycling, which requires further understanding and may be due to the formation of a stable SEI layer as well as consumption of $AlPO_4$ on the cathode surface at high voltage. The bulk-sensitive fluorescence yield (FLY) spectra of AlP-10 and bare LNMO before and after cycling are shown in Fig. S11 to further

understand the structure stability of bare and coated LNMO. The spectrum of cycled LNMO is not as similar as the pristine one, indicating the structure of LNMO may destroyed by side-reaction to inner of electrode without protection of coating layer. However, the spectra of bulk AlP-10 exhibits subtle changes after cycling, which suggests the $AlPO_4$ coating layer successfully helps to maintain LNMO cathode structure during cycling. Combining the results of electrochemical characterizations, ALD $AlPO_4$ coating layer can effectively protect Mn element from dissolution and maintains the integrity of LNMO during cycling.

To further understand the evolution of ultrathin ALD $AlPO_4$ coating layer, synchrotron based X-ray photoelectron spectra (XPS) of $AlPO_4$ coated LNMO electrodes before and after 50 charge/discharge cycles is employed and shown in Fig. 7. Prior to electrochemical cycling, Al 2p spectrum of AlP-10 is shown in Fig. 7a. Al-O bond is contributed to the formation of ALD $AlPO_4$ coating layer on the surface of LNMO. After cycling, the main peak of Al-O bond is also attributed to $AlPO_4$, while part $AlPO_4$ transfer to Al_2O_3. This may be due to the decomposition of $AlPO_4$ during cycling at high voltage [58]. The P 2p spectra of AlP-10 samples before and after charge/discharge cycles are shown in Fig. 7c and d. Before cycling, the peak of AlP-10 in P 2p spectrum can be assigned to the tetrahedral (PO_4)-group [59]. After cycling, the peak of the discharged AlP-10 was more complicated to form phosphorus-containing species (including PF_3 and PF_xO_y), which may be due to the decomposition of electrolyte or PO_4^{3-} during cycling [59,60]. Combined with synchrotron based XANES and XPS results, it can be predicted
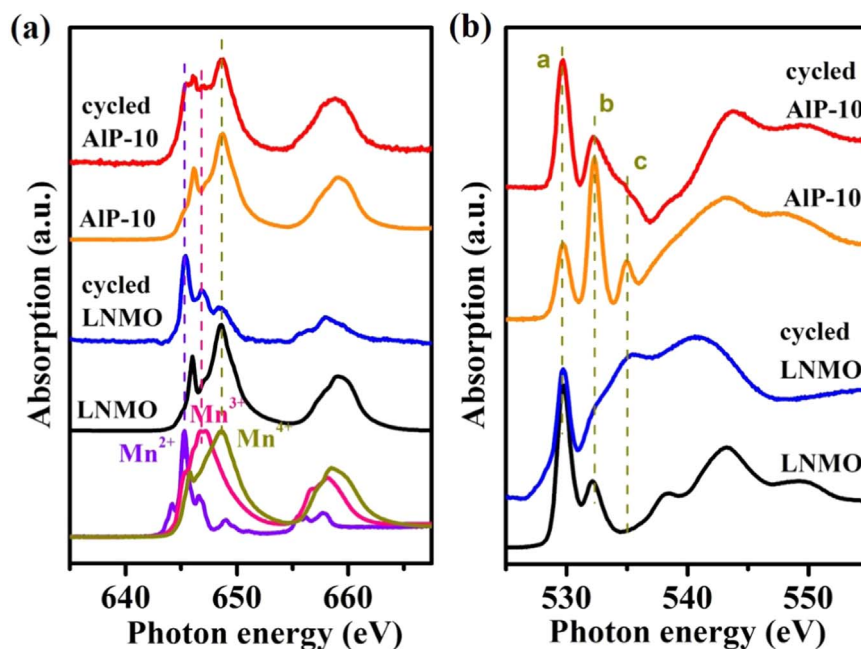

Fig. 6. (a) XANES Mn $L_{3,2}$-edges spectra of AlP-10 and LNMO before and after cycling with standard MnO, Mn_2O_3, MnO_2 as references; (b) XANES O K-edges of AlP-10 and LNMO before and after cycling.
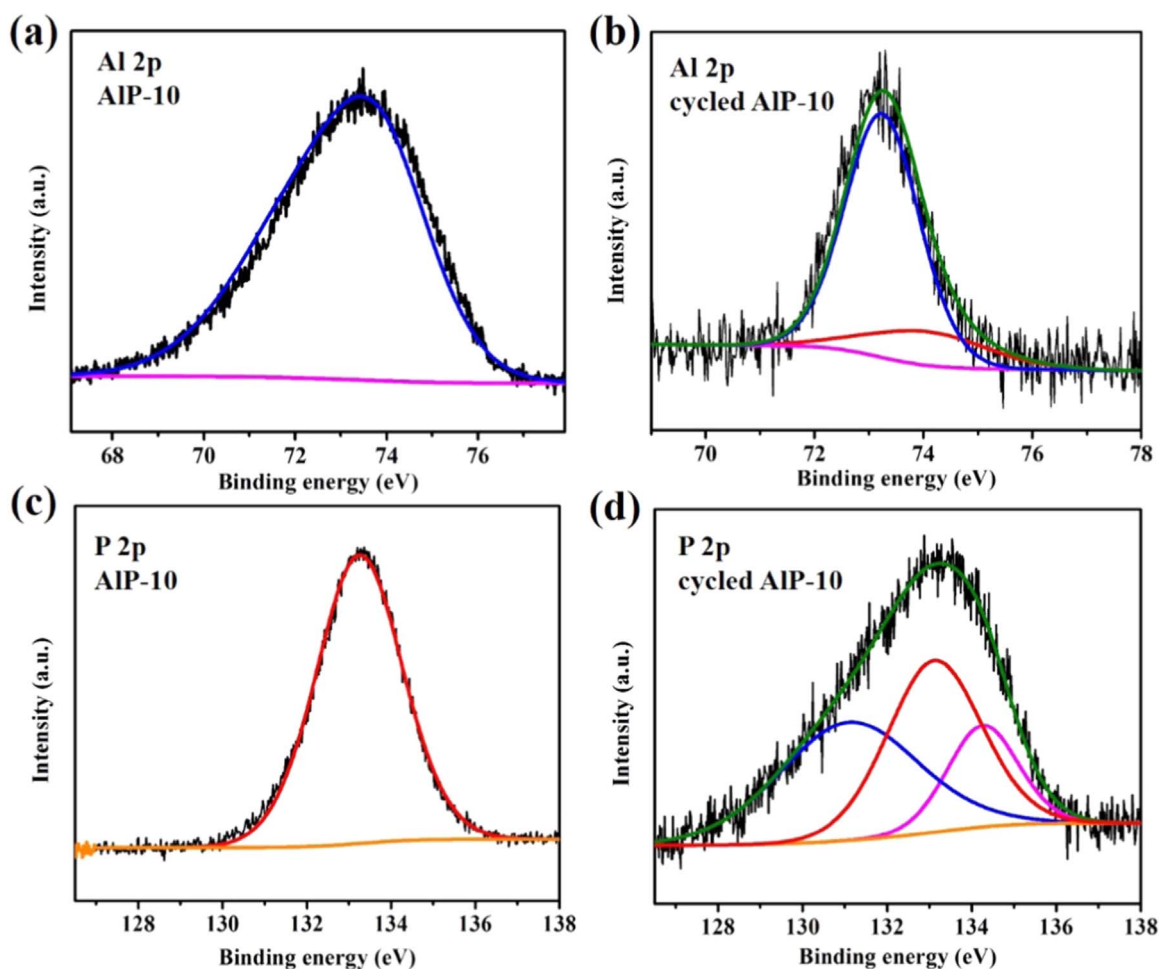
Fig. 7. (a-b) Al 2p XPS spectra and (c-d) P 2p XPS spectra of AlP-10 before and after cycling.

that the ALD AlPO$_4$ coating is not only an inhibitor to separate LNMO and electrolyte. During the charge/discharge process, this coating layer can be transferred into a stable SEI layer and help to maintain the structure of LNMO at the interphase, leading to enhanced cycling capacity of cells.

To demonstrate the thermal stability of ALD AlPO$_4$ coated LNMO, differential scanning calorimetry (DSC) tests of as-prepared LNMO electrodes with electrolyte in charge stage are carried out under N$_2$ atmosphere. As mentioned before, metastable Li$_x$NiMnO at charged stage aggravates the exothermal side-reactions with flammable electrolyte, leading to serious safety concerns. Therefore, especially at high voltage, thermal stability of LNMO in a charge state is critical for battery safety. As shown in Fig. 8, an exothermic peak indicates the value of heat generation (related to oxygen generation) from the decomposed electrode material following reaction with the electrolyte [29,61]. Bare LNMO electrode has a main exothermic peak at 217.6 °C. In contrast, the main exothermic peak of AlP-10 is shifted to 225.2 °C and displays a minimal thermal effect compared to bare LNMO (67% heat generation of bare LNMO). This result suggests that the AlPO$_4$-coating layer on the surface of LNMO stabilizes the interphase of LNMO and electrolyte with repressed side-reactions, effectively improving the safety of LNMO cells at high voltage operation.

Based on above results, the schematic diagram of the protecting role of AlPO$_4$ is presented in Fig. 9. It has been demonstrated that the uniform ALD AlPO$_4$ coating layer as an artificial SEI provides a stable interface between LNMO electrode and electrolyte, effectively suppressing the occurrence of side-reactions and dissolution of TMs. Additionally, the amorphous AlPO$_4$ layer can provides smooth Li$^+$ ion diffusion during charge/discharge cycling. Our work demonstrates
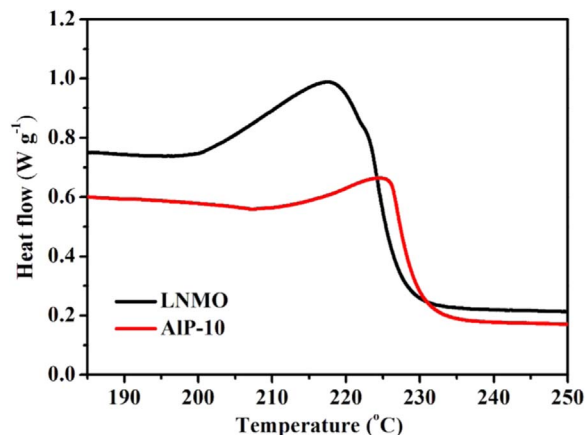

Fig. 8. DSC profiles of bare LNMO and AlP-10 cells charged at 5 V.

that AlPO$_4$ coating layer as a stable protective layer for high voltage cathode significantly improved safety and electrochemical performances of LIBs.

4. Conclusions

In summary, ultrathin ALD AlPO$_4$ film was employed as a coating material for high voltage LNMO cathode to enhance the electrochemical stability and the safety of Li-ion batteries. Our study demonstrated that 10 ALD-cycles of AlPO$_4$ coating on LNMO has the best long cycling performance. Synchrotron based XANES and XPS study were carried
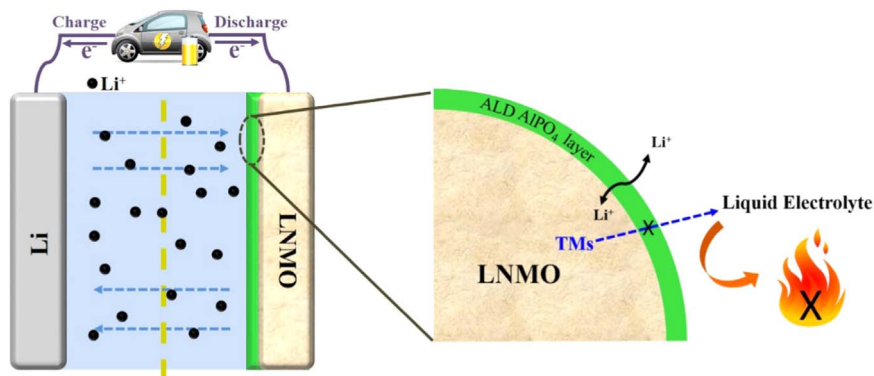
Fig. 9. Schematic diagram of the protecting role of ALD AlPO₄ coating on LNMO electrode.

out to understand the mechanism of modification on the surface of LNMO. The AlPO₄ coating layer was shown to effectively suppress dissolution of Mn and maintains the integral structure of LNMO. We proposed that the ultrathin ALD AlPO₄ coating layer acts not only as a barrier layer to separate LNMO and electrolyte, but also transforms into a stable SEI layer during cycling, effectively preventing electrolyte decomposition and protecting LNMO structure during electrochemical reaction. Finally, thermal stability of LNMO cathode materials was investigated via DSC analysis, further demonstrating enhanced safety properties of LNMO with AlPO₄ coating. The ALD AlPO₄ coating in this research addresses a long-time concerned issue of high voltage cathodes in Li-ion batteries, and can be applied for other energy storage systems following this design.

Acknowledgements

Appendix A. Supplementary material

Supplementary data associated with this article can be found in the online version at doi:10.1016/j.nanoen.2017.05.007.

References

[1] A. Kraytsberg, Y. Ein-Eli, Adv. Energy Mater. 2 (2012) 922–939.
[2] D. Hong, Y. Guo, H. Wang, J. Zhou, H.-T. Fang, J. Mater. Chem. A 3 (2015) 15457–15465.
[3] A. Manthiram, K. Chemelewski, E.-S. Lee, Energy Environ. Sci. 7 (2014) 1339–1350.
[4] J. Li, L. Baggetto, S.K. Martha, G.M. Veith, J. Nanda, C. Liang, N.J. Dudney, Adv. Energy Mater. 3 (2013) 1275–1278.
[5] H. Deng, P. Nie, H. Luo, Y. Zhang, J. Wang, X. Zhang, J. Mater. Chem. A 2 (2014) 18256–18262.
[6] H.-B. Kang, S.-T. Myung, K. Amine, S.-M. Lee, Y.-K. Sun, J. Power Sources 195 (2010) 2023–2028.
[7] J.R. Dahn, E.W. Fuller, M. Obrovac, U. von Sacken, Solid State Ion. 69 (1994) 265–270.
[8] D.D. MacNeil, L. Christensen, J. Landucci, J.M. Paulsen, J.R. Dahn, J. Electrochem. Soc. 147 (2000) 970–979.
[9] A.D. Pasquier, F. Disma, T. Bowmer, A.S. Gozdz, G. Amatucci, J.M. Tarascon, J. Electrochem. Soc. 145 (1998) 472–477.
[10] J.-H. Cho, J.-H. Park, M.-H. Lee, H.-K. Song, S.-Y. Lee, Energy Environ. Sci. 5 (2012) 7124–7131.
[11] J. Xu, Y. Hu, T. liu, X. Wu, Nano Energy 5 (2014) 67–73.
[12] G.B. Zhong, Y.Y. Wang, Y.Q. Yu, C.H. Chen, J. Power Sources 205 (2012) 385–393.
[13] J. Xiao, X. Chen, P.V. Sushko, M.L. Sushko, L. Kovarik, J. Feng, Z. Deng, J. Zheng, G.L. Graff, Z. Nie, D. Choi, J. Liu, J.-G. Zhang, M.S. Whittingham, Adv. Mater. 24 (2012) 2109–2116.
[14] L. Xiao, J. Xiao, X. Yu, P. Yan, J. Zheng, M. Engelhard, P. Bhattacharya, C. Wang, X.-Q. Yang, J.-G. Zhang, Nano Energy 16 (2015) 143–151.
[15] R. Santhanam, B. Rambabu, J. Power Sources 195 (2010) 5442–5451.
[16] D.R. Vissers, D. Isheim, C. Zhan, Z. Chen, J. Lu, K. Amine, Nano Energy 19 (2016) 297–306.
[17] J. Chong, S. Xun, X. Song, G. Liu, V.S. Battaglia, Nano Energy 2 (2013) 283–293.
[18] M. Xu, L. Zhou, Y. Dong, Y. Chen, J. Demeaux, A.D. MacIntosh, A. Garsuch, B.L. Lucht, Energy Environ. Sci. 9 (2016) 1308–1319.
[19] J.W. Kim, D.H. Kim, D.Y. Oh, H. Lee, J.H. Kim, J.H. Lee, Y.S. Jung, J. Power Sources 274 (2015) 1254–1262.
[20] J.C. Arrebola, A. Caballero, L. Hernán, J. Morales, J. Power Sources 195 (2010) 4278–4284.
[21] Y. Fan, J. Wang, Z. Tang, W. He, J. Zhang, Electrochim. Acta 52 (2007) 3870–3875.
[22] H.M. Wu, I. Belharouak, A. Abouimrane, Y.K. Sun, K. Amine, J. Power Sources 195 (2010) 2909–2913.
[23] W. Wen, X. Yang, X. Wang, L.G.H. Shu, J. Solid State Electrochem. 19 (2015) 1235–1246.
[24] H.-B. Kang, S.-T. Myung, K. Amine, S.-M. Lee, Y.-K. Sun, J. Power Sources 195 (2010) 2023–2028.
[25] Y. Kobayashi, H. Miyashiro, K. Takei, H. Shigemura, M. Tabuchi, H. Kageyama, T. Iwahori, J. Electrochem. Soc. 150 (2003) A1577–A1582.
[26] D. Liu, Y. Bai, S. Zhao, W. Zhang, J. Power Sources 219 (2012) 333–338.
[27] F. Wu, X. Zhang, T. Zhao, L. Li, M. Xie, R. Chen, ACS Appl. Mater. Interfaces 7 (2015) 3773–3781.
[28] J. Cho, H. Kim, B. Park, J. Electrochem. Soc. 151 (2004) A1707–A1711.
[29] G.-R. Hu, X.-R. Deng, Z.-D. Peng, K. Du, Electrochim. Acta 53 (2008) 2567–2573.
[30] J. Cho, J.-G. Lee, B. Kim, B. Park, Chem. Mater. 15 (2003) 3190–3193.
[31] J. Cho, J. Power Sources 126 (2004) 186–189.
[32] J. Cho, Y.-W. Kim, B. Kim, J.-G. Lee, B. Park, Angew. Chem. Int. Ed. 42 (2003) 1618–1621.
[33] J.-H. Wang, Y. Wang, Y.-Z. Guo, Z.-Y. Ren, C.-W. Liu, J. Mater. Chem. A 1 (2013) 4879–4884.
[34] J. Cho, T.-J. Kim, J. Kim, M. Noh, B. Park, J. Electrochem. Soc. 151 (2004) A1899–A1904.
[35] J.Y. Shi, C.-W. Yi, K. Kim, J. Power Sources 195 (2010) 6860–6866.
[36] Y. Wu, A. Vadivel Murugan, A. Manthiram, J. Electrochem. Soc. 155 (2008) A635–A641.
[37] X. Meng, X.-Q. Yang, X. Sun, Adv. Mater. 24 (2012) 3589–3615.
[38] C. Marichy, M. Bechelany, N. Pinna, Adv. Mater. 24 (2012) 1017–1032.
[39] X. Li, A. Lushington, Q. Sun, W. Xiao, J. Liu, B. Wang, Y. Ye, K. Nie, Y. Hu, Q. Xiao, R. Li, J. Guo, T.-K. Sham, X. Sun, Nano Lett. 16 (2016) 3545–3549.
[40] J. Liu, X. Sun, Nanotechnology 26 (2015) 024001.
[41] X. Li, J. Liu, M.N. Banis, A. Lushington, R. Li, M. Cai, X. Sun, Energy Environ. Sci. 7 (2014) 768–778.
[42] B. Xiao, J. Liu, Q. Sun, B. Wang, M.N. Banis, D. Zhao, Z. Wang, R. Li, X. Cui, T.-K. Sham, X. Sun, Adv. Sci. 2 (2015) 1500022.
[43] H.-M. Cho, M.V. Chen, A.C. MacRae, Y.S. Meng, ACS Appl. Mater. Interfaces 7 (2015) 16231–16239.
[44] M. Kunduraci, G.G. Amatucci, J. Electrochem. Soc. 153 (2006) A1345–A1352.
[45] C. Zhu, C.-G. Han, T. Akiyama, RSC Adv. 5 (2015) 49831–49837.
[46] J. Zheng, J. Xiao, X. Yu, L. Kovarik, M. Gu, F. Omenya, X. Chen, X.-Q. Yang, J. Liu, G.L. Graff, M.S. Whittingham, J.-G. Zhang, Phys. Chem. Chem. Phys. 14 (2012) 13515–13521.
[47] Y. Qian, Y. Deng, L. Wan, H. Xu, X. Qin, G. Chen, J. Phys. Chem. C 118 (2014) 15581–15589.
[48] C.Y. Xu, P.X. Zhang, L. Yan, J. Raman Spectrosc. 32 (2001) 862–865.
[49] Y.S. Lee, W.K. Shin, A.G. Kannan, S.M. Koo, D.W. Kim, ACS Appl. Mater. Interfaces

7 (2015) 13944–13951.
[50] T. Liu, A. Garsuch, F. Chesneau, B.L. Lucht, J. Power Sources 269 (2014) 920–926.
[51] N.P.W. Pieczonka, Z. Liu, P. Lu, K.L. Olson, J. Moote, B.R. Powell, J.-H. Kim, J. Phys. Chem. C 117 (2013) 15947–15957.
[52] J. Demeaux, D. Lemordant, H. Galiano, M. Caillon-Caravanier, B. Claude-Montigny, Electrochim. Acta 116 (2014) 271–277.
[53] U. Boesenberg, M. Falk, C.G. Ryan, R. Kirkham, M. Menzel, J. Janek, M. Fröba, G. Falkenberg, U.E.A. Fittschen, Chem. Mater. 27 (2015) 2525–2531.
[54] C. Zhan, J. Lu, A. Jeremy Kropf, T. Wu, A.N. Jansen, Y.-K. Sun, X. Qiu, K. Amine, Nat. Commun. 4 (2013) 2437.
[55] R. Qiao, L.A. Wray, J.-H. Kim, N.P.W. Pieczonka, S.J. Harris, W. Yang, J. Phys. Chem. C 119 (2015) 27228–27233.
[56] J. Zhou, D. Hong, J. Wang, Y. Hu, X. Xie, H. Fang, Phys. Chem. Chem. Phys. 16 (2014) 13838–13842.
[57] J. Ma, B. Li, L. An, H. Wei, X. Wang, P. Yu, D. Xia, J. Power Sources 277 (2015) 393–402.
[58] E. Markevich, R. Sharabi, H. Gottlieb, V. Borgel, K. Fridman, G. Salitra, D. Aurbach, G. Semrau, M.A. Schmidt, N. Schall, C. Bruenig, Electrochem. Commun. 15 (2012) 22–25.
[59] S. Verdier, L. El Ouatani, R. Dedryvère, F. Bonhomme, P. Biensan, D. Gonbeau, J. Electrochem. Soc. 154 (2007) A1088–A1099.
[60] Y.-C. Lu, A.N. Mansour, N. Yabuuchi, Y. Shao-Horn, Chem. Mater. 21 (2009) 4408–4424.
[61] X. Ma, C. Wang, X. Han, J. Sun, J. Alloy. Compd. 453 (2008) 352–355.
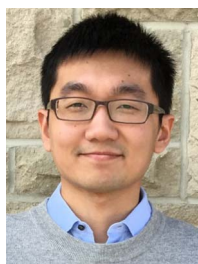
Sixu Deng is currently a Ph.D. candidate in Prof. Hao Wang's group at Beijing University of Technology (BJUT), China. At the same time, he is a visiting student in Prof. Xueliang (Andy) Sun's Nanomaterials and Energy Group at University of Western Ontario, Canada. He received his bachelor of material science and engineering degree from BJUT in 2011. His research interests focus on lithium-ion batteries, atomic layer deposition and supercapacitors.

Biwei Xiao has just finished his Ph.D. degree in Prof. Xueliang (Andy) Sun's group at the University of Western Ontario. He earned his bachelor of engineering degree from Sichuan University (China) in 2011. His research interests are associated with the synthesis, modification and mechanism study of cathode materials for lithium-ion batteries, atomic layer deposition, synchrotron radiation technique and carbonaceous materials.

Biqiong Wang is currently a Ph.D. candidate in Prof. Xueliang (Andy) Sun's Nanomaterials and Energy Group at Western University, Canada. She received her Bachelor degree in Materials Science in 2012 at the City University of Hong Kong. Her research interests are associated with the application of atomic layer deposition in all-solid-state batteries. She is also co-supervised by Prof. T. K. Sham from Chemistry Department in Western University. Part of her work is related to the study of energy materials via synchrotron radiation.

Xia Li is a postdoctoral fellow in Prof. Xueliang (Andy) Sun's Nanomaterials and Energy Group. She received her Ph.D. degree at the University of Western Ontario, Canada. Her current research interests focus on development of advanced nanomaterials for lithium-sulfur batteries, sulfur-based solid-state electrolyte.

Karthikeyan Kaliyappan received Bachelor of technology (B.Tech, 2005) and Master of technology (M.Tech, 2007) in Electrochemical Engineering from Central Electrochemical Research Institute, India. After completing masters, he worked as Junior Research Fellow in materials technology division, Central Power Research Institute, India from October 2007 to February 2009. He earned Ph.D. at Chonnam National University, South Korea in Advanced Chemicals and Engineering (2013). He is currently working as a postdoctoral fellow at the University of Waterloo, Waterloo, Canada. His current fields of interests are developing high energy density materials for energy storage devices including Li-ion and Na-ion batteries.

Yang Zhao is currently a Ph.D. candidate in Prof. Xueliang (Andy) Sun's Group at the University of Western Ontario, Canada. He received his B.S. degree and M.S. degree in Chemical Engineering and Technology from Northwestern Polytechnical University (Xi'an, China) in 2011 and 2014, respectively. His current research interests focus on atomic layer deposition in the application of lithium/sodium ion batteries and all solid state batteries.

Andrew Lushington is currently a Ph.D. candidate in prof. Xueliang (Any) Sun's Nanomaterials and Energy Group at the University of western Ontario. He received his BSc in Chemistry with a Concentration in Nanotechnology and a minor in Religion from Carleton University (Ottawa, Canada) in 2012. His current research interest is predominantly in the area of atomic and molecular layer deposition for the application and use in energy storage and energy conversion devices.

Ruying Li is a research engineer in Prof. Andy Xueliang Sun's group at the University of Western Ontario, Canada. She received her master degree in materials chemistry in 1999 from the University of Manchester, UK. Then she worked as a research assistant at the University of British Columbia, Canada and L'Institut National de la Recherche Scientifique (INRS), Canada. Her current research interests are focused on advanced materials and characterization for electrochemical energy storage and conversion, including electrocatalysis in fuel cells and electrodes in lithium batteries.

T.K. Sham is a Distinguished University Professor and a Canada Research Chair in Materials and Synchrotron Radiation at the University of Western Ontario. He obtained his Ph.D. from the University of Western Ontario (1975) with a BSc from the Chinese University of Hong Kong. He joined the Chemistry Department at Brookhaven National Laboratory in 1977 and returned to Western in 1988. He is presently the Director of the Soochow-Western Centre for Synchrotron Radiation, a Fellow of the Royal Society of Canada and an Officer of the Order of Canada. Dr. Sham's expertise are nanomaterial synthesis, surface and interface, X-ray absorption related spectroscopy and microscopy. His recently focus is nanostructure phase transition, assembly of nanocomposites, in situ/in operando studies of energy materials and devices. X-ray excited optical luminescence in the energy and time domain, nanomaterials for drug delivery, and micro-beam analysis of cultural and heritage materials.

Hao Wang is the professor in College of Materials Science and Engineering, Beijing University of Technology, China. Dr. Wang received his Ph.D. in applied chemistry in 1997 from Beijing Institute of Technology, China. Then he worked as a postdoctoral fellow in the Tokyo Institute of Technology, Japan. His current research interests are focused on advanced materials for electrochemical energy storage, and electrochromic materials and devices.

Xueliang (Andy) Sun is a Canada Research Chair in Development of Nanomaterials for Clean Energy, Fellow of the Royal Society of Canada and Canadian Academy of Engineering and Full Professor at the University of Western Ontario, Canada. Dr. Sun received his Ph.D. in materials chemistry in 1999 from the University of Manchester, UK, which he followed up by working as a postdoctoral fellow at the University of British Columbia, Canada and as a Research Associate at L'Institut National de la Recherche Scientifique (INRS), Canada. His current research interests are focused on advanced materials for electrochemical energy storage and conversion, including electrocatalysis in fuel cells and electrodes in lithium-ion batteries and metal-air batteries.